Scientia Iranica B (2014) 21(4), 1367–1377

SCIENTIA IRANICA

Sharif University of Technology
Scientia Iranica
Transactions B: Mechanical Engineering
www.scientiairanica.com

A finite volume method to investigate flow characteristics of an orifice pulse tube refrigerator

A.A. Boroujerdi[a,*] and S. Jafari[b]

a. *Faculty of Mechanical Engineering, K.N. Toosi University of Technology, Tehran, P.O. Box 19395-1999, Iran.*
b. *Department of Mechanical Engineering, Iran University of Science and Technology (IUST), Narmak, Tehran, 16844, Iran.*

Received 27 May 2012; received in revised form 7 December 2013; accepted 25 January 2014

KEYWORDS
Pulse tube;
Enthalpy flow;
Oscillatory flow;
Second order upwind;
Lagrangian approach.

Abstract. A finite volume method is developed for simulation of oscillatory compressible flow in the pulse tube part of an orifice pulse tube refrigerator. Governing equations for control volumes are written in 1D discretized form. Second order upwind is used for the convective terms as well as Euler implicit method for temporal derivatives. The results include the temperature and mass flow rate as functions of time and position, and the buffer pressure as a function of time. A typical pulse tube is modeled by using the numerical model. The results show that the present numerical method has good agreement with previously published results. The cold end (inlet) mass flow rate makes an angle of 39.60 with the pressure vector. Hot end mass flow rate is in phase with the pressure vector. Previously, it was mentioned that in one-dimensional models, overshoots never disappear completely, whereas in the present one-dimensional model they are eliminated. The overshoots in the both ends for present results are less than those for 3D results. By using the results of Eulerian coordinate, Lagrangian approach is used to track the movement of the gas parcels to get their pressure, temperature, and velocity in a thermodynamic cycle.

1. Introduction

The invention of the orifice pulse tube cooler is regarded as the milestone of the developments of pulse tube cooler. Since then, cooling performance of the PTCs has been significantly improved [1,2], which is now comparable to the conventional cryocoolers. Many theoretical analytical methods as well as numerical models have been developed to investigate the mechanism of refrigeration and intrinsic loss.

A zeroth order (thermo-dynamical) analysis gives overall knowledge of occurred phenomena in PTCs. Thermodynamical models [3-5] use the laws of thermodynamics to analyze the performance of a pulse tube. These thermodynamical models are based on time-averaged values.

Several attempts have been made to linearize the conservation laws. One of the possible approaches is harmonic analysis (see [6,7]). Harmonic time dependence is used and all variables of the system are expanded in the harmonic series. Subsequently, the 1D conservation equations are solved through an expansion series solution. One of the main benefits of this approach is its capability to perform rapid optimizations with respect to dimensions and operational conditions of the pulse tube cooler. However, this approach is restricted to small-amplitude harmonic pressure variations in the system.

Due to the complexity of the conservation equations, analytical solutions are basically impossible. This is why numerical models are of great importance.

*. *Corresponding author. Tel: +98 9112574025; Fax: +98 21 88677274*
E-mail addresses: A.A.Boroujerdi@gmail.com (A.A. Boroujerdi); S.Jafari87@gmail.com (S. Jafari)

In [8], a one-dimensional numerical model was used to describe an orifice-type pulse-tube refrigerator. All components of the system in this study were considered considering the basic assumptions: Ideal gas, ideal heat exchangers, and negligible axial heat conduction as well. Besides, the conservation equations were solved using the finite volume method. In later works [9,10], real gas properties were taken into account. The same model was used by Ju et al. [11] for studying a double-inlet pulse tube and a good agreement with experimental data was reported.

A two-dimensional model for the tapered tube section of a pulse tube refrigerator has been proposed in [12-14]. Linearized conservation equations were solved analytically. The effects of operating frequency, taper angle, and displacement volume ratio and phase angle between velocities at the ends of the tube on the net energy flow were studied.

The commercially available CFD code, such as Fluent [15], is a beneficial tool to numerically solve Navier-Stokes equations with the finite volume discretization scheme. Some researchers have demonstrated the application of CFD simulations to PTRs. The multidimensional flow effect has been analyzed by Cha and Ghiaasiaan [16] on a high frequency inertance tube pulse tube. In fact, they modeled the regenerator and all heat exchangers as porous media taking the gas viscous and inertial losses into account. Barrett and Arsalan [17] performed a CFD simulation of a stirling type simple OPTR using an axis-symmetric model. In their model the regenerator and the pulse tube have the same radius. The conclusion was that a three-dimensional modeling tends to be very time consuming and consequently not applicable for real system optimization. In this paper, a one-dimensional numerical method is developed for simulation of flow and thermal field of the pulse tube part of an orifice pulse tube refrigerator.

2. Physical model and governing equations

2.1. Physical model and assumptions

A schematic of an orifice pulse tube refrigerator is shown in Figure 1. Assumptions considered are as follows:

1. Ideal Newtonian gas;
2. One-dimensional laminar flow;
3. Negligible viscous dissipation;
4. No external force;
5. Constant wall temperature with respect to the time.

In pulse tube cryocoolers, Mach number is small. However, compressibility cannot be neglected because of density changes induced by the driving pressure. This kind of flow is called low Mach number compressible flow.

The experimental results show that the onset of turbulence in oscillating flow is different from that in steady flow. The critical transition parameter is a Reynolds number based on the Stokes layer thickness, δ,

$$\mathrm{Re}_\delta = \frac{\bar{u}\delta}{\nu}, \tag{1}$$

$$\delta = \sqrt{\frac{2\nu}{\omega}}. \tag{2}$$

By using experimental results, the stability-plane has been defined for oscillating pipe flow in the "Re_δ versus r/δ" space. According to this stability-plane, turbulence occurs if $\mathrm{Re}_\delta > 500$. For the present pulse tube parameters, we have $\mathrm{Re}_\delta = 230$, which is in the perturbed-laminar flow region.

Considering an Eulerian point of view, the flow field unknowns can then be described as the functions $\dot{m}(x,t)$, $P(x,t)$, $\rho(x,t)$ and $T(x,t)$. The spatial domain of the pulse tube is divided to n finite volumes. Thus there are $n+1$ faces as shown in Figure 2. Solid circles ($1 \leq I \leq n$) store the nodal values of the temperature, pressure, density, mass, and gas properties. The cross signs ($1 \leq i \leq n+1$) are the storage locations for the nodal values of the mass flow rate, velocity, enthalpy flow, energy flow, and the exergy flow. This staggered arrangement of finite volumes helps to prevent non-physical numerical solutions in the Finite Volume Method (FVM).

2.2. Governing equations

Based on the mentioned assumptions, the governing equations are:

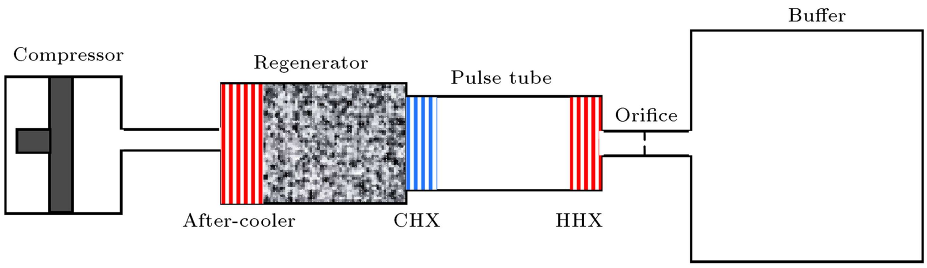

Figure 1. Schematic of an orifice pulse tube refrigerator.

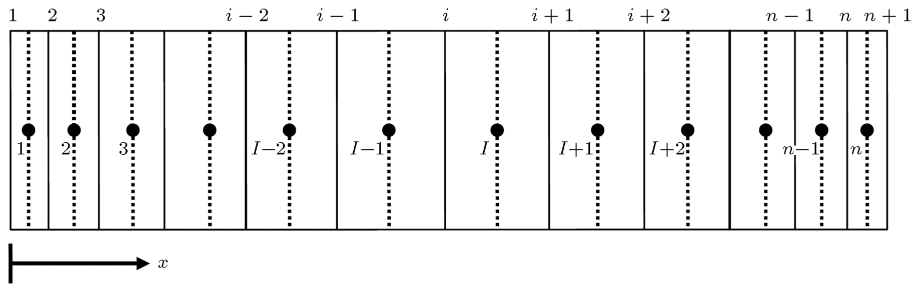

Figure 2. Subdivided domain of the pulse tube.

Continuity equation:

$$\frac{\partial \rho}{\partial t}+\frac{\partial(\rho u)}{\partial x}=0. \tag{3}$$

Conservation of momentum equation:

$$\frac{\partial(\rho u)}{\partial t}+\frac{\partial(\rho u^2)}{\partial x}=-\frac{\partial P}{\partial x}-f_F. \tag{4}$$

The last term of momentum equation is implemented to describe wall-flow interaction which is equivalent to the integration of viscous terms of 2-D Navier-Stokes equations over a cross section of the tube.

Conservation of energy equation:

$$\frac{\partial}{\partial t}\left(\rho\frac{u^2}{2}+\rho C_V T\right)+\frac{\partial}{\partial x}\left(\rho u\frac{u^2}{2}+\rho u C_P T+\dot{q}\right)=0. \tag{5}$$

Unlike momentum equation, here, the interaction between gas and wall has been neglected because of its complexity (non-synchronicity of heat transfer and temperature difference). Also, it is negligible in comparison to enthalpy flow.

State equation of the gas:

$$PV=mRT. \tag{6}$$

Integrating of the above differential equations over an arbitrary finite volume gives:

$$\frac{\partial m_I}{\partial t}=\dot{m}_i-\dot{m}_{i+1}, \tag{7}$$

$$\frac{\partial}{\partial t}(mu)_i=(\dot{m}u)_{I-1}-(\dot{m}u)_I+A(P_{I-1}-P_I)-\frac{8\mu_i}{\rho_i r^2}\delta x\,|\dot{m}_i|, \tag{8}$$

$$\frac{\partial}{\partial t}\left(m\frac{u^2}{2}+mC_V T\right)_I=\left(\dot{m}\frac{u^2}{2}+\dot{m}C_P T+\dot{q}\right)_i-\left(\dot{m}\frac{u^2}{2}+\dot{m}C_P T+\dot{q}\right)_{i+1}. \tag{9}$$

2.3. Initial conditions

Real initial conditions in the pulse tube are zero velocity, the charge (not mean) pressure, and the ambient temperature. To reach to an oscillatory steady state solution in a computer program needs very long CPU time (several days). Whereas oscillatory steady solution is essential to have a deep insight in analyzing pulse tube refrigerator, it is efficient to consider an initial guess solution close to steady values instead of real initial condition. The chosen initial conditions are:

$$P(x,0)=P_m,$$
$$\dot{m}(x,0)=0,$$
$$T(x,0)=(T_{hhx}-T_{chx})x/L+T_{chx}. \tag{10}$$

Furthermore, a linear initial condition for temperature field is assumed. In [18], three profiles (linear, exponential, and step function) have been considered to investigate the effect of initial conditions.

3. Numerical simulation

3.1. Procedure of the continuity and momentum equations

In the momentum equation, the temporal derivative of the momentum can be changed to the temporal derivative of the mass flow rate as:

$$\frac{\partial}{\partial t}(mu)_i=\frac{\partial}{\partial t}(\rho_i A\delta x u_i)=\delta x\frac{\partial \dot{m}_i}{\partial t}. \tag{11}$$

The momentum flow at the nodes is calculated by second order upwind:

$$(\dot{m}u)_I=\begin{cases}u_I(1.5\dot{m}_i-0.5\dot{m}_{i-1}) & u_I\geq 0\\ u_I(1.5\dot{m}_{i+1}-0.5\dot{m}_{i+2}) & u_I<0\end{cases} \tag{12}$$

To deal with pressure force, combine state equation of the gas with continuity equation, and then approximate the temporal derivative by using the Euler implicit method. Thus a relation which gives pressure at the nodes explicitly is derived:

$$P_I^k=(\dot{m}_i^k-\dot{m}_{i+1}^k)\delta t\frac{RT_I^k}{V}+P_I^{k-1}\frac{T_I^k}{T_I^{k-1}}. \tag{13}$$

The index k shows the value at the present time level, and index $k-1$ shows the values at previous time level.

The density is replaced by state equation of the gas. The pressure at faces is estimated by central linear interpolation:

$$P_i = \frac{1}{2}(P_{I-1} + P_I). \tag{14}$$

Finally, inserting Eqs. (6), and (11)-(13) into the momentum equation (8), gives:

$$\begin{aligned}
&\frac{\delta x}{\delta t}(\dot{m}_i^k - \dot{m}_i^{k-1}) + \max(u_I^k, 0)(1.5\dot{m}_i^k - 0.5\dot{m}_{i-1}^k) \\
&\quad + \min(u_I^k, 0)(1.5\dot{m}_{i+1}^k - 0.5\dot{m}_{i+2}^k) \\
&\quad - \max(u_{I-1}^k, 0)(1.5\dot{m}_{i-1}^k - 0.5\dot{m}_{i-2}^k) \\
&\quad - \min(u_{I-1}^k, 0)(1.5\dot{m}_i^k - 0.5\dot{m}_{i+1}^k) \\
&\quad + (\dot{m}_i^k - \dot{m}_{i+1}^k)\frac{\delta t R T_I^k}{\delta x} + A P_I^{k-1}\frac{T_I^k}{T_I^{k-1}} \\
&\quad - (\dot{m}_{i-1}^k - \dot{m}_i^k)\frac{\delta t R T_{I-1}^k}{\delta x} - A P_{I-1}^{k-1}\frac{T_{I-1}^k}{T_{I-1}^{k-1}} \\
&\quad + \frac{8\mu\delta x}{r^2}\frac{RT_i}{P_i}\dot{m}_i^k = 0.
\end{aligned} \tag{15}$$

The aforementioned equation along with boundary conditions are solved by Penta-Diagonal Matrix Algorithm.

3.2. Boundary conditions of the momentum equation

3.2.1. The left boundary (cold end, $x = 0$)

It has a sinusoidal or trapezoidal pressure, corresponds to a specified mean value and amplitude. For sinusoidal oscillation, we have:

$$P_{i=1} = P_m + P_a \sin(2\pi f t). \tag{16}$$

Combining Eqs. (13), (14) and (16) gives an equation which includes the inlet mass flow rate.

3.2.2. The right boundary (hot end, $x = L$)

It is at the orifice face if the resistive effect of the hot heat exchanger is neglected. The gas velocity at the hot end is proportional to the pressure difference between two sides of the orifice, i.e. buffer pressure and hot end pressure given as:

$$u_H = \frac{C_{or}}{A}(P_H - P_b). \tag{17}$$

Eq. (17) can be easily changed to derive an equation for mass flow rate. To do this, the buffer pressure must be specified. The volume of the buffer is large compared to that of the pulse tube, typically being 10 times larger. One procedure is that the pressure in the buffer is considered nearly constant and practically equal to the average pressure in the system. A more accurate procedure is a time dependent buffer pressure, so an extra equation is needed. It is the conservation of mass equation for the buffer:

$$\frac{\partial}{\partial t}\left(\frac{P_b V_b}{R T_b}\right) = \dot{m}_H = C_{or}\rho_H(P_H - P_b). \tag{18}$$

Two common ways to deal with the thermal behavior of the gas inside the buffer are assuming isothermal and adiabatic process. The first assumption is considered in this study. The temperature of the buffer is almost constant during the oscillation process and equals to the temperature of the hot heat exchanger which is the same as ambient temperature. As a result, the conservation of the mass equation for the buffer can be written as:

$$\frac{\partial P_b}{\partial t} = C_{or}\rho_{i=n+1}(P_{i=n+1} - P_b)\frac{R T_{hhx}}{V_b}. \tag{19}$$

By using the Euler implicit method, Eq. (19) would change to a simple algebraic equation:

$$P_b^k - P_b^{k-1} = \delta t C_{or}\rho_{i=n+1}(P_{i=n+1} - P_b)\frac{R T_{hhx}}{V_b}. \tag{20}$$

Inserting Eq. (20) into the last part of Eq. (18) gives the mass flow rate at the hot end as the right boundary condition.

3.3. Procedure of energy equation

To evaluate a convection-dominated problem, the upwind scheme for the enthalpy flow and temperature at faces is commonly used.

Because of large temperature gradient, the second order upwind method is used. The temperature at the faces is derived as:

$$T_i = \begin{cases} 1.5T_{I-1} - 0.5T_{I-2}^k & \dot{m}_i^k \geq 0 \\ 1.5T_I^k - 0.5T_{I+1}^k & \dot{m}_i^k < 0 \end{cases} \tag{21}$$

Similarly, the enthalpy flow at the faces is estimated as:

$$(\dot{m}C_P T)_i = \begin{cases} \dot{m}_i C_P(1.5T_{I-1} - 0.5T_{I-2}) & \dot{m}_i \geq 0 \\ \dot{m}_i C_P(1.5T_I - 0.5T_{I+1}) & \dot{m}_i < 0 \end{cases} \tag{22}$$

The heat conduction rate is calculated by Fourier's law as:

$$\dot{q}_i = -kA\left[\frac{\partial T}{\partial x}\right]_i = -kA\frac{T_I - T_{I-1}}{\delta x}. \tag{23}$$

Temporal derivatives of energy equation are discretized by the Euler implicit method. Finally, the energy equation of the gas is obtained in the following form:

$$\begin{aligned}
&\frac{P_I^k V C_V}{R T_I^k \delta t} T_I^k + \max(\dot{m}_{i+1}^k C_P, 0)(1.5T_{I+1}^k - 0.5T_{I+2}^k) \\
&\quad + \min(\dot{m}_{i+1}^k C_P, 0)(1.5T_I^k - 0.5T_{I-1}^k) \\
&\quad - \max(\dot{m}_i^k C_P, 0)(1.5T_I^k - 0.5T_{I+1}^k) \\
&\quad - \min(\dot{m}_{i+1}^k C_P, 0)(1.5T_{I-1}^k - 0.5T_{I-2}^k) \\
&\quad + kA\frac{T_I^k - T_{I-1}^k}{\delta x} - kA\frac{T_{I+1}^k - T_I^k}{\delta x} \\
&\quad = \frac{P_I^{k-1} V C_V}{R \delta t} + 0.5\Bigg(\frac{P_I^k V (u_I^k)^2}{R T_I^k \delta t} \\
&\quad - \frac{P_I^{k-1} V (u_I^{k-1})^2}{R T_I^{k-1} \delta t} + \dot{m}_{i+1}^k (u_{i+1}^k)^2 \\
&\quad - \dot{m}_i^k (u_i^k)^2\Bigg). \qquad (24)
\end{aligned}$$

The above equation along with boundary conditions are solved by Penta-Diagonal Matrix Algorithm.

3.4. Boundary conditions of the energy equation

3.4.1. The left boundary (cold end, $x = 0$)

At the left boundary and while flow is positive (inflow to the domain), temperature is equal to constant temperature of the cold heat exchanger. When flow is negative (outflow), temperature is calculated by using the second order upwind approximation, thus:

$$T_{i=1} = \begin{cases} T_{chx} & \dot{m}_i^k \geq 0 \\ 1.5T_I^k - 0.5T_{I+1}^k & \dot{m}_i^k < 0 \end{cases} \qquad (25)$$

3.4.2. The right boundary (hot end, $x = 0$)

This boundary is treated similar to the left boundary, therefore:

$$T_{i=n+1} = \begin{cases} 1.5T_{I-1} - 0.5T_{I-2}^k & \dot{m}_i^k \geq 0 \\ T_{hhx} & \dot{m}_i^k < 0 \end{cases} \qquad (26)$$

3.5. Solution algorithm

The following procedure is used for the calculation process:

1. Enter parameters including dimensions (length and diameter), gas properties, performance parameters (such as frequency, mean pressure, and flow conductance of orifice), and options (number of iterations per time step, time steps per cycle, number of cycles, and number of control volumes).
2. Guess initial values for mass flow rate, pressure and temperature.
3. Calculate the mass flow rates.
4. Calculate the pressure field explicitly.
5. Calculate velocities and temperatures at the faces.
6. Calculate the temperature field.
7. Iterate steps 3 through 6 until one time step ends.
8. Go to the next time step.
9. Repeat steps 3 to 8 for a specified number of the cycles.

4. Results and discussion

4.1. Input parameters

A typical pulse tube is modeled by using the aforementioned numerical model. The geometry, gas (Helium) properties, and performance conditions are taken from [19] which are listed in Table 1. Optional parameters, which are used for simulation, are tabulated in Table 2.

4.2. Flow field

In the most studies, the pressure gradient in the pulse tube was neglected. Figure 3 shows the pressure distribution on the pulse tube at the half and end of

Table 1. Physical data.

Parameter	Value-unite
C_{or}	10^{-8} m^3.Pa^{-1}.s^{-1}
C_p	5197 J.Kg^{-1}.K^{-1}
C_v	3120 J.Kg^{-1}.K^{-1}
f	20 Hz
k	0.158 W.m^{-1}.K^{-1}
L	0.2 m
P_m	3 MPa
P_a	0.5 MPa
r	0.025 m
R	2077 J.Kg^{-1}.K^1
T_H	300 K
T_C	70 K
V_b	0.005 m^3
μ	2.0e-5 Pa.s

Table 2. Optional parameters.

Number of control volumes	100
Number of time steps per cycle	100
Number of cycles	200

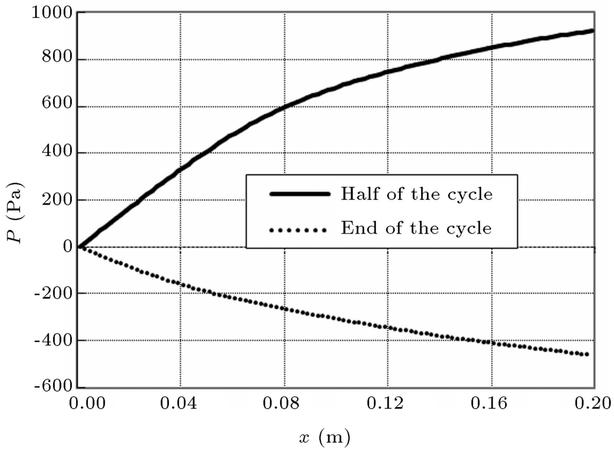

Figure 3. Pressure distribution at half and end of the 200th cycle.

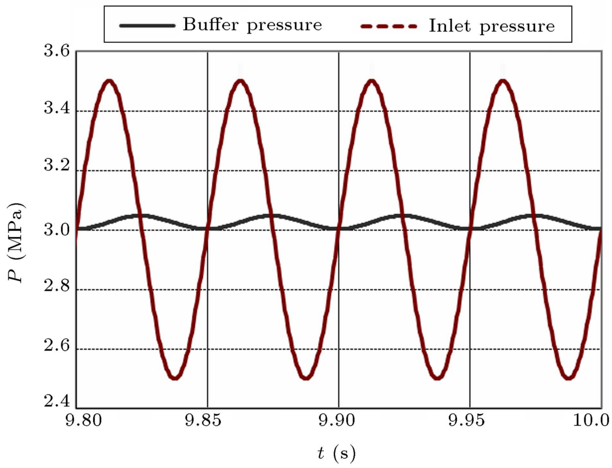

Figure 4. Inlet pressure and buffer pressure.

the 200th cycle. The pressure drop in the pulse tube is less than 1 kPa.

A larger buffer volume gives smaller amplitude of the buffer pressure. Variations of the inlet pressure and the buffer pressure are shown in Figure 4. It is obvious that the buffer pressure has a phase lag produced by the orifice. The mean value of the buffer pressure (3.0252 MPa) is approximately as same as the buffer pressure calculated by analytical treatment:

$$P_b = \sqrt{P_m^2 + P_a^2/2} = 3.0208 \text{ MPa}. \tag{27}$$

The temporal variations of inlet and outlet mass flow rates and driving pressure (minus mean value) as crucial parameters are shown in Figure 5. This figure shows that the cold end (inlet) mass flow rate makes an angle of 39.6° with pressure vector. The refrigeration power is proportional to the product of the inlet mass flow rate and pressure. Hot end mass flow rate is in phase with the pressure vector, because the orifice always provides a flow on the hot end of the pulse tube which is in phase with the pressure.

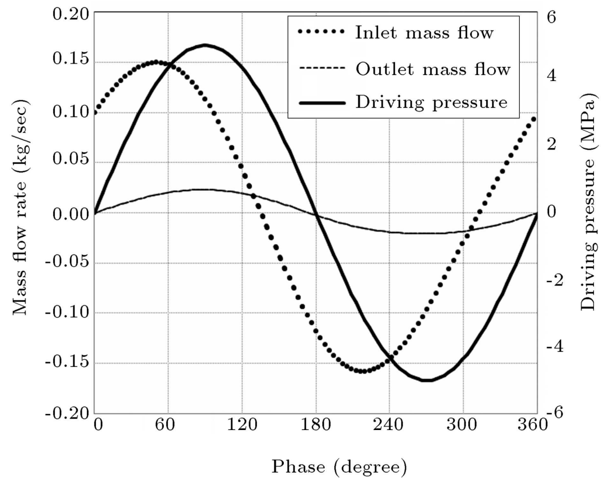

Figure 5. The temporal variations of inlet and outlet mass flow rates and driving pressure in the last cycle.

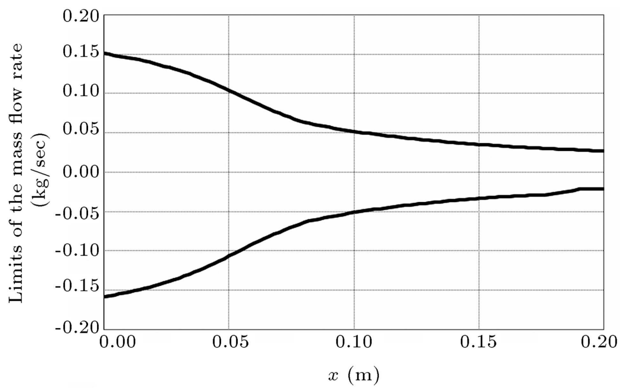

Figure 6. Limits (maximum and minimum) of the mass flow rate.

According to Figure 6, where the limits (maximum and minimum) of the mass flow rate are shown, it can be found that the relative change in mass flow rate is approximately 82%.

4.3. Temperature field

Temperature of cold and hot ends of the pulse tube along with the results achieved by harmonic treatment [5] and 3D simulation [20] is shown in Figure 7. In the half-cycle, where the velocity at cold end of the pulse tube is positive (gas flows from CHX into pulse tube) based on upwind approximation, temperature at the cold end of the pulse tube is equal to the temperature of the cold heat exchanger, and is constant. On the other hand, in the half-cycle, where the velocity at the cold end of the pulse tube is negative, temperature at the cold end arises corresponding to mass flow rate variations. These results can be found by comparing Figures 5 and 6. Besides, there is a similar behavior for the temperature at the hot end of the pulse tube.

The results show that the present numerical method has a good agreement with previous results.

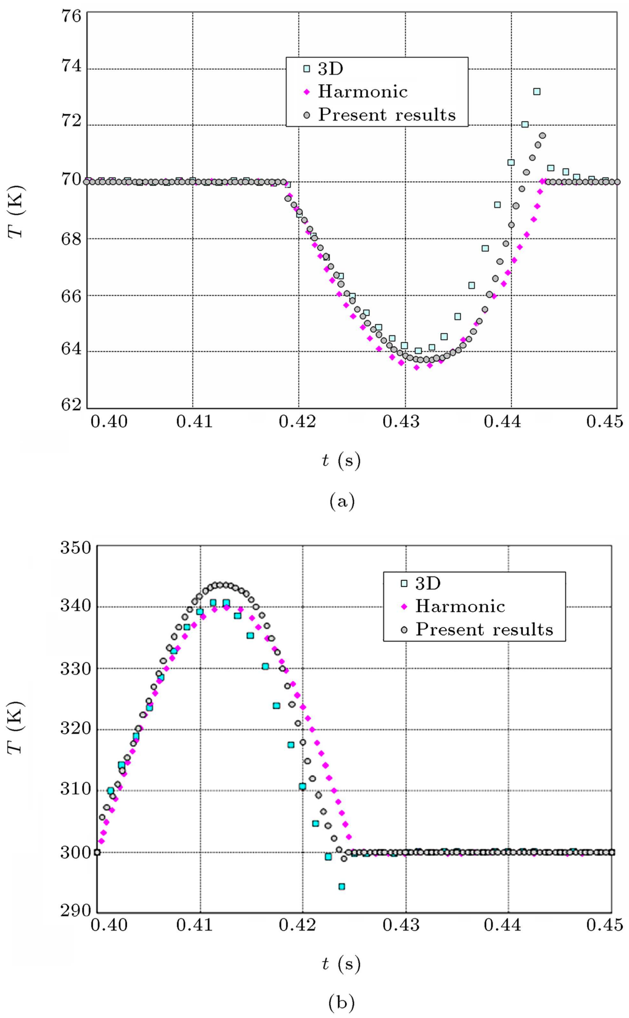

Figure 7. Temperatures of cold and hot ends in 9th cycle: (a) Cold end; and (b) hot end.

Also overshoots at both ends for present results are less than that for 3D results. These overshoots were being reported also in other one-dimensional simulations and that is because of a small net gas flow in the system. Overshoots are sensitive to the velocity and temperature boundary conditions, the initial conditions, and the grid refinement. It was reported that in previous one-dimensional models, overshoots never disappeared completely [19], whereas in the present one-dimensional model they are eliminated after 40 and 12 cycles for cold and hot end (Figures 8 and 9.), respectively. Furthermore, they disappear sooner than 2D model [19] which is based on finite difference method.

Temperature of gas in 100th cycle obtained by the present model, and 1D and 2D results of Lyulina's simulation are shown in Figure 10. In Figure 10(a), the effect of upstream cold temperature in the cold region is clear. Besides, the temperature rising in Figure 10(b) is due to the effect of gas compression in the hot region.

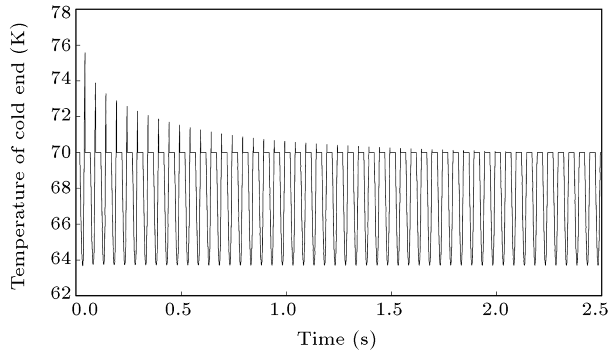

Figure 8. Temperature at cold end in first 50 cycles.

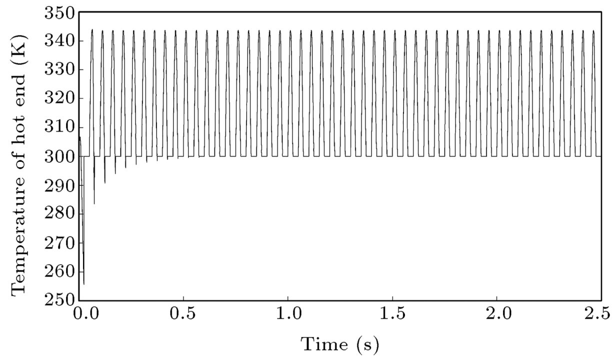

Figure 9. Temperature at hot end in first 50 cycles.

4.4. Energy flow and enthalpy flow

After calculation of the mass flow rate, velocity, temperature, and pressure, total parameters are obtained. Total parameters are mean cyclic values of net mass flow rate, enthalpy flow, and energy flow. When cyclic (periodic) steady state is reached, net mass flow rate over a cycle must be zero based on the continuity equation.

However, this condition is never satisfied because of numerical errors. To evaluate numerical errors during cycles, mean cyclic mass flow rate is named as "error" (28). After 200 cycles, error reaches to 1.6×10^{-6} kg/s that is very satisfactory. Figure 11 shows the error during 200 cycles.

Another important total parameter is the enthalpy (sum of internal energy and flow work) flow (29). The energy flow is the sum of enthalpy flow, kinetic energy, and heat conduction of the gas (30). Ideally, the energy flow is equal to the cooling power of the cooler. When the periodic steady state is reached, integration of the energy equation over one cycle implies that energy flow must be constant along the pulse tube. Therefore, the energy flow and enthalpy flow are suitable criterion for investigation of the convergence of the solution. Figure 12 shows the net cyclic enthalpy and energy flows of 200th cycle in the pulse tube. From Figure 12, it is clear that net cyclic energy flow in the pulse tube is not constant and varies a little during cycles.

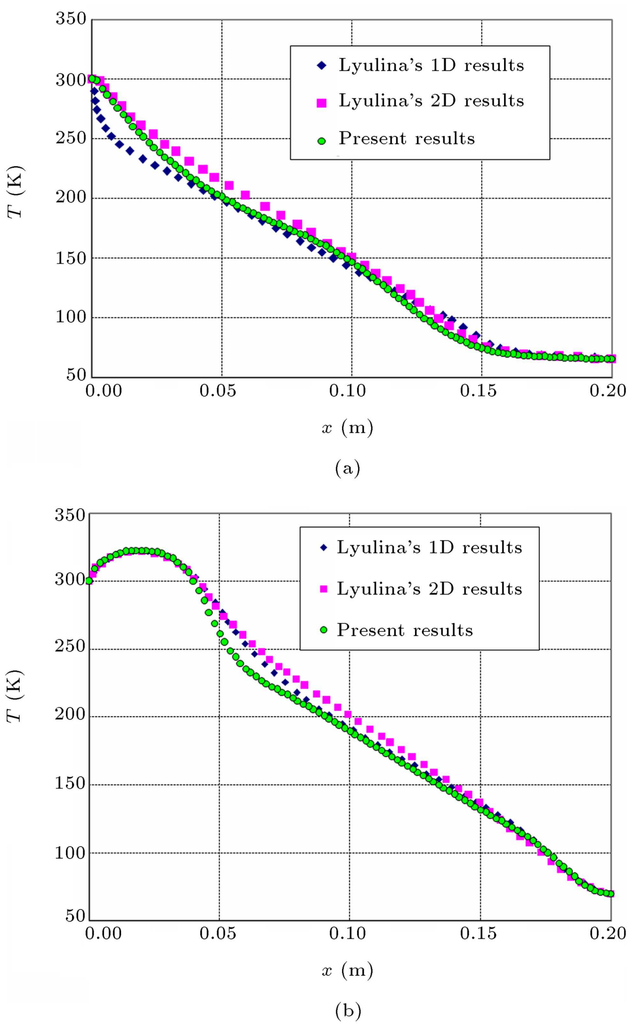

Figure 10. Temperature at half and end of 100th cycle: (a) $t = 4.975$ s; and (b) $t = 5.000$ s.

$$e = \frac{1}{n+1} \sum_{i=1}^{n+1} \frac{1}{\tau} \oint \dot{m}_i dt, \tag{28}$$

$$\bar{\dot{H}} = \frac{1}{\tau} \oint \dot{m} C_P T dt, \tag{29}$$

$$\bar{\dot{E}} = \frac{1}{\tau} \oint \left[\dot{m} \left(C_P T + \frac{u^2}{2} \right) - kA \frac{\partial T}{\partial x} \right] dt. \tag{30}$$

Also, a $G-M$ type pulse tube cryocooler, which has a trapezoidal driving pressure, is simulated by using the numerical model. The enthalpy flow calculated by present simulation for sinusoidal and trapezoidal inlet pressure has been compared to analytical results in Table 3. The difference between the present results and the analytical results is less than 1

4.5. Lagrangian approach

After numerical calculations, summarizing the obtained results in Lagrangian view, the quantitative results of thermodynamic cycles will come out. In [21],

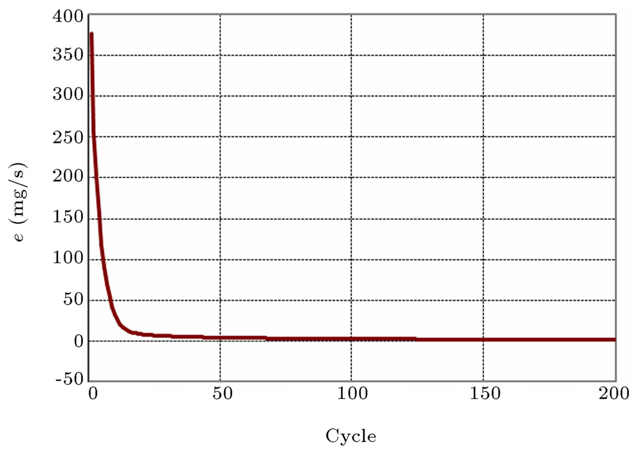

Figure 11. Error of net mass flow rate during cycles.

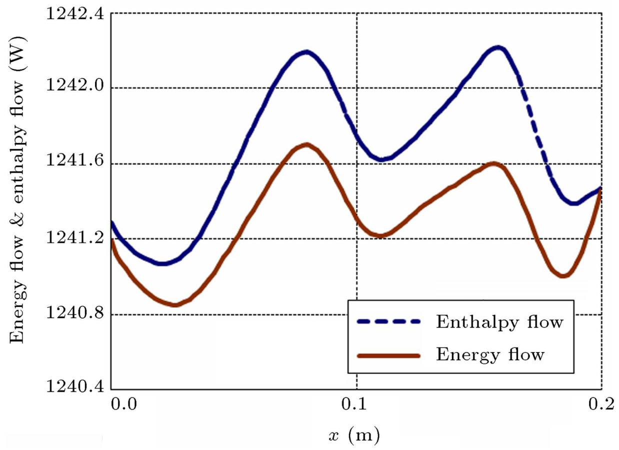

Figure 12. Energy flow and enthalpy flow of 200th cycle along pulse tube.

Table 3. Net enthalpy flow (watts) for two different types of pressure oscillations.

Inlet pressure	Analytical estimation	Present results
Sinusoidal	1250	1242
Trapezoidal	1944	1925

the mixed Eulerian-Lagrangian method was applied to simulate and visualize one-dimensional gas flow in a two-stage pulse-tube cooler which is operating in the 4 K temperature region. A moving grid is used to follow the exact tracks of gas particles (Lagrangian approach) when they move with pressure oscillation in the pulse tube. For the regenerator, a mixed computational grid was used (Eulerian approach). Using calculated values of 200th cycle in Eulerian coordinate, an additional Lagrangian approach is used to track the movement of a gas parcel to get its pressure, temperature, and velocity at different positions in a thermodynamic cycle. Assuming constant velocity of the gas parcel during a time step, the gas parcel would move to a new certain position at a new time level. If the new position is not located in a grid point, pressure, temperature, and velocity of the gas parcel are calculated by linear interpolation of corresponding parameters at two adjacent grids. After 100 time steps calculations, the gas parcel would return to its original position. Therefore, complete thermodynamic cycles of the gas parcel can be obtained. Results show that different gas parcels undergo thermodynamic cycles at different temperatures. These gas parcels convey heat from the low temperature part to the high temperature part of the system.

Figure 13 shows the temperature of four gas particles in the pulse tube. Accordingly, the elements which are close to the cold end have more displacement and less temperature variations than those which are close to the hot end. Pressure of two gas particles in the pulse tube is depicted in Figure 14. For Stirling-type pulse tube, thermodynamic cycle of gas particles is an elliptical path as seen from $T - x$ diagram as well as in $P - x$ diagram shown in Figures 13 and 14, respectively. A $G - M$ type pulse tube cooler has nearly trapezoidal shape thermodynamic cycle. Four

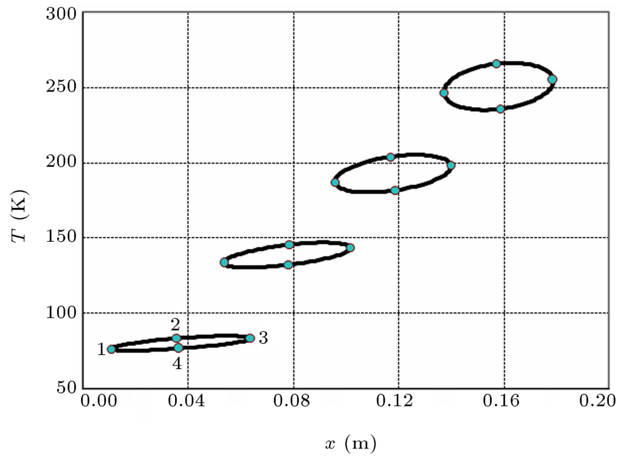

Figure 13. Temperature of gas particles during one cycle.

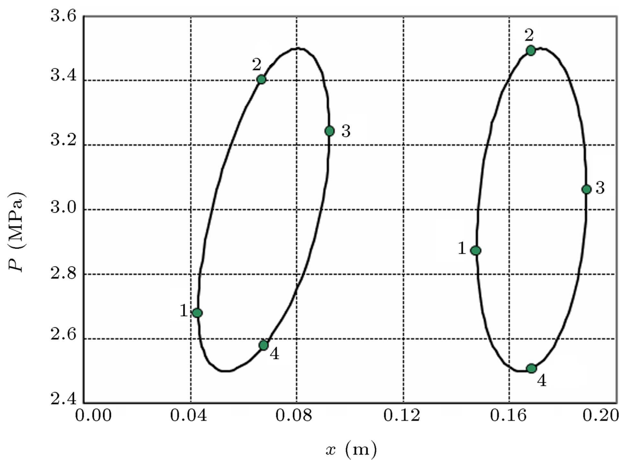

Figure 14. Pressure of gas particles during one cycle.

points are considered in thermodynamic cycle. Point 1 is selected as the starting point (left bound of gas position) of the cycle whose pressure is a little more than its minimum value and velocity is zero. Between points 1 and 2, gas particles move to the hot end and their velocity increases because of the acceleration produced by driving pressure. The pressure and temperature increase because of compression work which is done on gas column. At point 2, pressure is a little less than the maximum pressure, and the velocity is the maximum. From point 2 to point 3, gas particles move to the hot end. The velocity at point 3 is zero; hence point 3 is at the right bound of gas position. In the path between point 3 and point 4, the velocity increases because of expansion (negative acceleration). Besides, the temperature and the pressure decrease in this section. Point 4 has maximum absolute value of the velocity. From points 4 to 1 the velocity decreases insofar as it becomes zero at point 1.

5. Conclusion

A finite volume method is developed for the numerical simulation of oscillatory compressible flow in the pulse tube part of an orifice-type pulse tube refrigerator. Governing equations for control volumes are written in 1D discretized form. A staggered grid is used in the spatial domain. The second order upwind method is used for the convective terms as well as Euler implicit method for temporal derivatives. A typical pulse tube is modeled by using the numerical model. The results show that the present numerical method has a reasonable agreement with previous results. The results show that the pressure drop in the pulse tube is less than 1 kPa. It is found that the buffer pressure has a phase lag produced by the orifice. The mean value of the buffer pressure is approximately as same as buffer pressure calculated by analytical technique. The cold end (inlet) mass flow rate makes an angle of 39.6° with pressure vector. Hot end mass flow rate is in phase agreement with the pressure vector. Previously, it was mentioned that in one-dimensional models overshoots never disappear completely whereas in the present one-dimensional model they are eliminated. In addition, the overshoots in both ends for present results are less than those for 3D results. Furthermore, they disappear sooner than 2D model which was based on the finite difference method.

Calculation of the mass flow rate, velocity, temperature, and pressure leads to obtain total parameters. Total parameters are mean cyclic values of net mass flow rate, enthalpy flow, and energy flow. Also, a G-M type pulse tube cryocooler, which has a trapezoidal driving pressure, is simulated by using the numerical model. The enthalpy flow calculated by present simulation for sinusoidal and trapezoidal inlet pressure has been compared with analytical results. The one-dimensional numerical results differ nearly 1% from analytical results in two cases. Finally, by using the calculated values of 200th cycle in Eulerian coordinate, an additional Lagrangian approach is used to track the movement of a gas parcel to get its pressure, temperature, and velocity at different positions in a thermodynamic cycle.

Acknowledgement

The authors express their special thanks to Dr. A. Ashrafizadeh for his comments on the numerical solution.

Nomenclature

A	Cross sectional area of pulse tube
C_{or}	Flow conductance of orifice
C_p	Constant pressure specific heat capacity
C_v	Constant volume specific heat capacity
e	Error of the mass flow rate
$\bar{\dot{E}}$	Mean cyclic energy flow
f	Operating frequency
f_F	Friction force
$\bar{\dot{H}}$	Mean cyclic enthalpy flow
k	Thermal conductivity
L	Length of the pulse tube
m	Mass
$\dot{m}$	Mass flow rate
n	Number of control volumes
N	Total variable
P_a	Pressure oscillation amplitude
P_m	Mean pressure
$\dot{q}$	Heat conduction rate
r	Radius of the pulse tube
R	Gas constant
Re	Reynolds number
Re_δ	Reynolds number based on δ
T	Temperature
u	Velocity
$\bar{u}$	Amplitude of the velocity
V	Volume
x	Distance from cold end

Greel letters

δ	Stokes layer thickness
ω	Angular frequency
δt	Time step
δx	Spatial step
μ	Viscosity
ρ	Density
τ	Period
ν	Kinematic viscosity

Subscripts

b	Buffer
chx	Cold heat exchanger
H	Hot end
hhx	Hot heat exchanger
I	Node number
i	Face number

Superscripts

k	Time level number

References

1. Qiu, L.M., He, Y.L., Gan, Z.H. and Chen, G.B. "A single-stage pulse tube cooler reached 12.6 K", *Cryogenics*, **45**, pp. 641-643 (2005).
2. Zhang, X.B., Qiu, L.M., Gan, Z.H. and He, Y.L. "Effects of reservoir volume on performance of pulse tube cooler", *Int. J. Refrigeration*, **30**(1), pp. 11-18 (2007).
3. Steijaert, P.P. "Thermodynamical aspects of pulse-tube refrigerator", PhD Thesis, Eindhoven University of Technology (1999).
4. de Waele, A.T.A.M., Steijaert, P.P. and Gijzen, J. "Thermodynamical aspects of pulse tubes", *Cryogenics*, **37**(6), pp. 313-324 (1997).
5. de Waele, A.T.A.M., Steijaert, P.P. and Gijzen, J. "Thermodynamical aspects of pulse tubes II", *Cryogenics*, **38**(3), pp. 329-335 (1998).
6. Hooijkaas, H.W.G. and Benschop, A.A.J. "Pulse tube development using harmonic simulations", *Cryocoolers*, **10**, pp. 359-367 (1999).
7. de Waele, A.T.A.M. "Regenerator dynamics in the harmonic approximation", *Cryogenics*, **41**(3), pp. 195-200 (2001).
8. Wang, C., Wu, P. and Chen, Z. "Numerical modelling of an orifice pulse tube refrigerator", *Cryogenics*, **32**, pp. 785-790 (1992).
9. Wang, C. "Numerical analysis of 4K pulse tube coolers: Part 1. Numerical simulation", *Cryogenics*, **37**, pp. 207-213 (1997).
10. Wang, C. "Numerical analysis of 4K pulse tube coolers: Part 2. Performances and internal processes", *Cryogenics*, **37**, pp. 215-220 (1997).
11. Ju, Y.L., Wang, C. and Zhou, Y. "Numerical simulation and experimental verification of the oscillating flow in pulse tube refrigerator", *Cryogenics*, **38**, pp. 169-176 (1998).

12. Baek, S.H., Jeong, E.S. and Jeong, S. "Two-dimensional model for tapered pulse tubes. Part 1: Theoretical modeling and net enthalpy flow", *Cryogenics*, **40**, pp. 379-385 (2000).

13. Baek, S.H., Jeong, E.S. and Jeong, S. "Two-dimensional model for tapered pulse tubes. Part 2: Mass streaming and streaming-driven enthalpy flow loss", *Cryogenics*, **40**, pp. 387-392 (2000).

14. Park, H.C., Jeong, E.S. and Jeong, S. "Two-dimensional model for tapered pulse tubes. Part 3: Unsteady components of second-order mass flux and temperature", *Cryogenics*, **42**, pp. 485-493 (2002).

15. Fluent 6 user manual, Fluent Inc, pp. 8-11 (2003).

16. Cha, J.S. and Ghiaasiaan, S.M. "Multi-dimensional flow effects in pulse tube refrigerators", *Cryogenics*, **46**, pp. 658-665 (2006).

17. Barrett, F. and Arsalan, R. "Modeling pulse tube cryocoolers with CFD", *Adv. Cryo. Eng.*, **49**, pp. 1493-1499 (2004).

18. Lyulina, I., Mattheij, R.M.M., Tijsseling, A.S. and Waele, A.T.A.M., *Numerical Simulation of Pulse-Tube Refrigerators: 1D Model*, Eindhoven University of Technology, Eindhoven, The Netherlands (2004).

19. Lyulina, I. "Numerical simulation of pulse tube refrigerators", PhD Thesis, Eindhoven University of Technology, Eindhoven, The Netherlands (2004).

20. Willems, D.W.J. and Dam, J.A.M. "Three-dimensional pulse tube simulations", *Adv. Cryo. Eng.*, **47**, pp. 934-941 (2001).

21. Ju, Y.L., Wang, C. and Zhou, Y. "Computational study of a 4K two-stage pulse tube cooler with mixed Eulerian-Lagrangian method", *Cryogenics*, **41**, pp. 49-51 (2001).

Biographies

Ali Akbar Boroujerdi received MSc degree in Mechanical Engineering (Energy Conversion) from K.N. Toosi University of Technology (Tehran, Iran) with excellent grade in 2008. He has research experiences of power-plant industries, pulse tube cryocoolers, thermoacoustic engines, physics of sea water waves, flow in porous media, etc. In the fall of 2012, he has been admitted as a Ph.D. student in Mechanical Engineering at K.N. Toosi University of Technology.

Saeid Jafari is a graduated MSc student in the Mechanical Engineering Department of Iran University of Science and Technology. He worked on modeling and optimization in mechanical system with focus on thermal systems. His areas of expertise include Energy, Exergy and Environmental Modeling, CFD, HVAC, Experimental Fluid Dynamics and Genetic Algorithm optimization. He is the co-author of several journals and conference papers.